Journal of Applied Polymer Science

Cellulose Nanocrystal Driven Crystallization of Poly(D,L-lactide) and Improvement of the Thermomechanical Properties

Sandra Camarero-Espinosa,[1] Dylan J. Boday,[2] Christoph Weder,[1] E. Johan Foster[1,3]

[1]Adolphe Merkle Institute, University of Fribourg, Chemin des Verdiers 4, CH-1700 Fribourg, Switzerland

[2]IBM Materials Engineering, Tucson, Arizona 85744-0002

[3]Virginia Tech, Department of Materials Science and Engineering, 213 Holden Hall, 445 Old Turner Street, Blacksburg, Virginia 24061

Correspondence to: E. J. Foster (E-mail: johanf@vt.edu)

ABSTRACT: The technological exploitation of polylactide in fields requiring wide range of operating conditions is limited by the low crystallization rate of the polymer and therewith the low thermomechanical stability. Here we report the crystallization and consequent improvement of the thermomechanical properties of originally amorphous poly(D,L-lactide) (D : L ratio 11 : 89) loaded with cellulose nanocrystals (CNCs). Isothermal treatment of samples with different CNC contents and at various temperatures, showed up to 6 wt % crystalline phase formation, as confirmed by differential scanning calorimetry and X-ray diffraction measurements. Under a particular set of annealing conditions, CNCs promote the formation of a lamellar structure. This provides the system with higher order and cohesion which in combination with stress-transfer between CNCs, led to an increase of the storage modulus in the rubbery plateau up to 30 times (from 2.7 MPa up to 79 MPa), a rise of the melting temperature up to 50°C, and an improvement of the Young's modulus up to 40%. © 2014 Wiley Periodicals, Inc. J. Appl. Polym. Sci. **2015**, *132*, 41607.

KEYWORDS: cellulose and other wood products; crystallization; mechanical properties; nanoparticles; nanowires and nanocrystals

Received 10 September 2014; accepted 3 October 2014

DOI: 10.1002/app.41607

INTRODUCTION

Polymers from biorenewable sources are attracting increasing attention as "green" alternative to the classical oil-based materials.[1–4] These biopolymers have been successfully implemented in industry replacing some commodity polymers in applications where relatively low mechanical properties and thermal stability are required,[5–9] commonly referred to as disposable good applications. Although this sector represents a large percentage of the polymer annual consumption, biopolymers are only slowly entering other fields where higher mechanical properties are required, for example construction, electronic or automotive applications.

Lactic acid and lactide derived polymers are aliphatic polyesters with a high potential of replacing some engineering materials. Synthetized by ring-opening polymerization of the lactide or dimerization of the lactic acid and further polymerization, this already commercially available biopolymer has been exploited not only as a substitute of some commodities but also in biomedical applications where biodegradable and biocompatible materials are essential. Three forms of lactide are simultaneously synthesized, the LL-, DD-, and LD-stereoisomers, which upon polymerization give rise to stereocopolymers of different D : L ratios. Pure L- or D- homopolymers (PLLA or PDLA, respectively) are isotactic and therefore semicrystalline, but the introduction of one of the alternate stereoisomers into the polymer chain, even if a small amount (>8 wt %), results in an amorphous material. The stereoselective polymerization of lactides is therefore of great importance, but so far only complicated routes are available to overcome this problem.[10–12] Of course, the degree of crystallinity of the polymer has a significant influence on the mechanical and thermomechanical properties of the final material, and control over the crystallization rate and crystal size are therefore of great importance.[13]

Recently, significant efforts have been made to increase the crystallinity and the crystallization rate of poly(lactide) (PLA) homopolymers and copolymers by cold, hot, isothermal and non-isothermal methods.[14–16] Several crystal structures have been assigned to different crystallization conditions and polymer compositions. The most common α and α' forms have a pseudoorthorhombic unit cell containing two homopolymer chains.[17,18] These crystal structures are different only in the packing density, where the α form is more ordered and thermomechanically more stable than its counterpart α'. The α' form is

Additional Supporting Information may be found in the online version of this article.

formed mainly at crystallization temperatures below 100°C, while at temperatures between 100 and 120°C both, α and α' forms coexist. A second crystal structure, the orthorhombic β form composed of six chains,[18] was later reported by Eling et al.,[19] and found to be a consequence of tensile stress applied to melt-spun PLLA fibers. Ikada et al.[20] reported the formation of a stereocomplex between D- and L-homopolymer chains when these two stereopolymers were blended, and as a result the melting point was increased by 50°C. Moreover, in recent years, stereocomplex formation and the nucleation potential therein has been studied, appearing to be a viable approach for the crystallization of PLA.[21–23] More recently, Stoclet et al.[24,25] identified the formation of a mesophasic structure in poly (D,L-lactide) (P(D,L-LA)) copolymers with up to 4 wt % D-isomer content when drawn at 70°C for a minimum strain of 130%. This lamellar structure appeared to be mechanically more stable than other crystal forms.[26] Furthermore, the effects of compression induced stress were analyzed by Pluta et al.,[27] who showed the formation of a fibrillar structure in copolymers containing 30 wt % of the D-form.

To this point, research has been focused on the use of a variety of nucleating agents to accelerate the crystallization process and better control the crystal growth in polylactides. Nanocomposites of semicrystalline PLA and clay, carbon nanotubes, titanium oxide, silver, silica, iron oxide and cellulose have been investigated[4,28–33] showing an increase of the crystallization kinetics.

Cellulose nanocrystals (CNC) are an abundant, easily recoverable form of natural cellulose, with high on-axis stiffness (105–168 GPa[34–36]), and high aspect ratio. Different dimensions (5–50 nm diameter and 100–3000 length[34,35,37]) and surface functionalities can be obtained, depending on the source and the hydrolysis method employed, which makes CNCs a very interesting material in the bionanocomposite field.[38–41] The surface hydroxyl groups of cellulose nanocrystals interact through hydrogen bonds that can support the formation of a percolating CNC network in a polymer matrix.[41] Because of these outstanding mechanical properties CNCs have been exploited as reinforcing filler in a large variety of nanocomposites.[42–47]

Lately, Pei et al.[48] studied the effect of surface modified CNCs as nucleating agents and reinforcing fillers in PLA-based nanocomposites, improving the dispersability of those into the matrix and showing an increase of the crystallization kinetics and mechanical properties.[31,48–53] Nevertheless, in all these studies, semicrystalline PLLA was employed and no evidence of the formation of a mesophasic structure was detected. Here we report for the first time the ability of unmodified CNCs to promote the crystallization and lamellar structure formation of originally amorphous poly(D,L-lactide) containing 11 wt % of the D-form upon thermal treatment. An optimal annealing temperature and CNC content were found to induce the formation of the mesophase, leading to an increase of the mechanical properties above the glass transition temperature and an improvement of the thermomechanical stability of the final nanocomposite by up to 50°C. The enhancement of such a poly(D,L-lactide) via the combination of CNC reinforcement and lamella formation could allow for introduction of PLA in applications where cost is a major consideration as this copolymer is obtained with less controlled and thus less costly manufacturing procedure.

EXPERIMENTAL

Materials

Sulfuric acid and *N*,*N*-dimethylformamide (DMF) were purchased from Sigma–Aldrich and used as received. Poly(D,L-lactide) grade 4060D was bought from Natureworks LLC (MN, USA). The copolymer contains 11.4 mol % of the D-isomer in statistical distribution and has a density of 1.24 g cm^{-3}, as indicated by the supplier. Gel permeation chromatography (GPC) experiments were carried out and a molecular weight of 114,300 g mol^{-1} ($\pm$1.7%) and a polydispersity index of 1.7 ($\pm$2.9%) were calculated. Cellulose nanocrystals were extracted from Whatman No. 1 filter paper by sulfuric acid hydrolysis according to a well-established[41] protocol that represents a modification of the method of Dong et al.[54] CNCs were characterized by transmission electron microscopy, from which length and diameter were determined to be 204 ± 57 and 24 ± 5, respectively (Supporting Information Figures S1 and S2). Quantification of introduced surface sulfate groups was performed by conductometric titration and elemental analysis and determined to be of 100 ± 7 mmol kg^{-1} of cellulose (Supporting Information Figure S3) and 0.28 ± 0.02 wt % (87 ± 6 mmol kg^{-1}), respectively.

Nanocomposite Preparation

Nanocomposites of P(D,L-LA) and 0, 2, 10, or 17 wt % CNCs were prepared by solution casting. The polymer was dissolved in DMF at a concentration of 40 mg mL^{-1} by stirring at 70°C for 4 h. CNCs were separately dispersed in DMF at a concentration of 10 mg mL^{-1} by sonicating for 8 h in a bath sonicator with a continuous water flow (Sonoswiss SW3H, Sonoswiss AG, Ramsen, Switzerland). Aliquots of the CNC dispersion and the P(D,L-LA) solutions were mixed by stirring and cast into Teflon® Petri dishes; the amounts were chosen so that the total solid content was 2 g per sample and to adjust the CNC content in the range quoted above. For example, 45 mL of the polymer solution were mixed with 20 mL of the CNC dispersion, stirred, and cast to prepare a 2 g nanocomposite film containing 10 wt % CNCs. DMF was then evaporated in an oven in which the sample was placed for 3 days at 70°C. Dry films were recovered from the Petri dishes and compression-molded between Teflon® sheets in a Carver press at 140°C and 7000 psi of pressure for 5 min to erase the thermal history. The resulting films were then annealed at temperatures between 80 and 140°C for 90 min under 7000 psi for crystallization experiments. The thickness of the films was controlled by spacers to reach a typical value of 150–200 μm as measured with the calliper. Removal of the solvent was checked by thermogravimetrical analyses (TGA) of the nat and CNC loaded samples as compared to neat CNC samples. Data are shown in Supporting Information Figure S5.

Differential Scanning Calorimetry (DSC)

The thermal properties of the nanocomposites were studied by DSC using a DSC 1 Star^e System (Mettler-Toledo GmbH, Geissen, Germany) equipped with a Huber TC 100 immersion

cooler (Peter Huber Kältemaschinenbau GmbH, Offenburg, Germany). Samples of 15–20 mg of nanocomposite film were cut and analyzed in a temperature cycle (20°C min^{-1}) consisting of a first heating from −50 to 250°C followed by a cooling from 250 to −25°C and a second heating to reach a final temperature of 300°C, where degradation of the samples was observed. Melting and glass transition temperatures of annealed samples were determined from the initial scan. Cooling and second heating scans were employed to check the integrity of the pristine material (without thermal history).

X-ray Diffraction (XRD)

Diffractograms were recorded with a Rigaku Ultima IV (Rigaku Europe SE, Ettlingen, Germany) equipped with a Cu Kα radiation source ($\lambda = 1540$ A) operating at 40 kV. Pure CNC samples (~150 mg) were ground in a mortar with a pestle (Caution: this should be done with proper protection measures to avoid inhalation of the CNCs), dissolved in 1 mL of water and dried in the oven at 100°C for 30 min. These pure CNC films were later reground and transferred to quartz holders. Here, the more compact samples were flattened to cover the whole analysis window reducing the air content. Neat polymer and nanocomposite film samples of about 30 × 30 mm^2 were taped into quartz sample holders covering the entire window. Diffractograms were recorded over a 2θ range of 5–60°. Spectra were deconvoluted using MagicPlot software (www.magicplot.com). A background subtraction (second order curve) was followed by fitting of peaks using Gaussian curves. Peaks of neat cellulose were fitted taking into account only cellulose type I and were left free for intensity and position and HWHM. Cellulose I diffraction peaks[55,56]: (101): 14.7° (10ī): 16.8° (021): 20.6° (002): 22.5° (040): 34.7°.

The nanocomposite spectra were normalized to the cellulose (002) peak, assuming that all the films contain the same wt % of CNCs. HWHM of cellulose inside the polymer matrix was fixed using the parameter determined for pure cellulose experiments. The cellulose peaks associated with CNCs incorporated into the nanocomposite appear shifted by 1–2.5 2θ degrees due to surface roughness effects of the nanocomposite film and crystallization of the copolymer. The position of cellulose peaks inside the polymer matrix was fixed using the following parameters:

(101): 16.1° (10 ī): 17.6° (021): 23.1° (002): 24.09° (040): 34.7°

Position of the amorphous halo in the nanocomposites was determined from a neat polymer sample, unadjusted for position, intensity and HWHM. Amorphous contribution of the polymer nanocomposites was then fixed to 16° 2θ and a HWHM of 2.4, as determined previously, without adjusting for intensity. Polymer peaks appeared sharp so they were fixed for position while HWHM and intensity were allowed to self-adjust.

Poly(D,L-lactide) diffraction peaks[57]: (103): 10.8° (200)/(110): 18.04° (203): 20.3° (210): 21.9

A new peak appeared at a 16.5° 2θ in all the annealed samples which was unadjusted for position, intensity and HWHM. In the three annealed samples, this peak appeared at a same position with the same HWHM, and was identified as a mesophasic peak.

Atomic Force Microscopy (AFM)

AFM images were recorded in air, on a JPK Nanowizard II equipped with a SPM Controller III (JPK Instruments AG, Berlin, Germany). Height and phase images were simultaneously recorded in tapping mode. Silicon nitrate coated cantilevers with a nominal spring constant of 42 N m^{-1} and a resonance frequency of 320 Hz were employed for all experiments (Nanoworld AG, Neuchâtel, Switzerland). Samples were prepared by attaching a 0.5 × 0.5 cm^2 piece of the nanocomposite onto a glass slide with double-sided tape.

Dynamic Mechanical Thermal Analysis (DMTA)

The thermomechanical properties of the nanocomposites and the neat copolymer were characterized by DMTA measurements that were conducted on a TA Q800 instrument (TA Instruments-Waters L.L.C., New Castle, DE). Rectangular samples of 30 × 6 mm^2 were cut from the nanocomposite and copolymer films and analyzed between 0 and 170°C with a heating rate of 3°C min^{-1}. A minimum of five samples were tested for each composition and annealing temperature. Frequency and strain amplitude (1 Hz and 15 μm) were kept constant during the entire experiment. Storage moduli (E') at 25 and 80°C were determined from these measurements and reported as an average ± standard deviation.

Tensile Testing

Tensile tests of the neat copolymer and the nanocomposites were carried out on a Zwick/Roell Z010 (Zwick GmbH & Co. KG, Ulm, Germany) test instrument equipped with tensile clamps and a 10 kN load cell. Samples with dimensions of 10 × 50 mm^2 were cut and tested applying a preload of 0.5N and a deformation ramp of 1 mm min^{-1}. The strain was increased until failure of the sample. The Young's modulus (E) was calculated from the linear region, between 0.2 and 0.4% strain. The yield strength was determined from the maximum of the strain-stress curve prior to plastic deformation. The ultimate strength was determined from the maximum strength reached in the plastic deformation region and the maximum strain was determined from the last point of the curve before fracture.

Optical Microscopy

Optical microscopy images were recorded on an Olympus BX51 microscope in transmission mode. The instrument was equipped with two linear polarizers (Olympus U-POT), which were used as indicated, and an Olympus DPT2 camera (Olympus Schweiz AG, Volketswil, Switzerland).

RESULTS AND DISCUSSION

Sample Preparation

P(D,L-LA)/CNC nanocomposites with a CNC content of 2, 10, or 17 wt % were prepared by solution casting from DMF. Before casting, sonication of CNCs for 8 h afforded a stable dispersion, with little observed nanoparticle aggregation in the corresponding nanocomposites. After drying, the materials were compression-molded at 140°C for 5 min and subsequently rapidly cooled to afford nanocomposite films with a thickness of 150–200 μm. Reference films of the neat P(D,L-LA) were

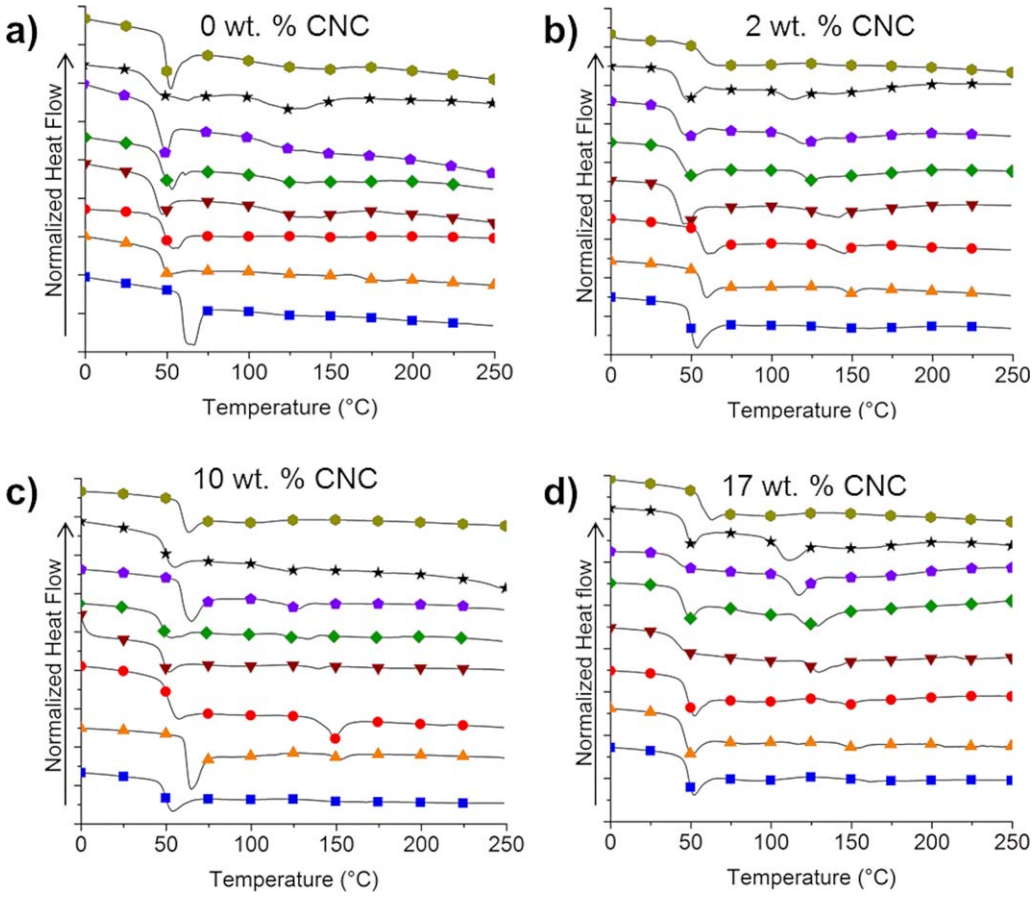

Figure 1. Differential scanning calorimetry (DSC) traces of neat P(D,L-LA) (a) and P(D,L-LA)/CNC nanocomposites containing 2 wt % (b), 10 wt % (c), or 17 wt % (d) CNCs. The samples are either quenched from the melt (⬢) or were annealed isothermally at 80 (★), 90 (⬟), 100 (◆), 110 (▼), 120 (•), 130 (▲) or 140°C (■) for 90 min. Shown are first heating scans that were normalized to the sample weight and acquired with a heating rate of 20°C min^{-1}. [Color figure can be viewed in the online issue, which is available at wileyonlinelibrary.com.]

prepared using the same process. The samples were then isothermally annealed under 7000 psi of pressure for 90 min in a hot press at 80, 90, 100, 110, 120, 130, or 140°C. Samples are coded X %Y°C, where X refers to the CNC content in wt % and Y indicates the annealing temperature. For example, the code for a sample with 10 wt % CNC annealed at 120°C is 10%120°C. Samples that were not annealed after quenching from the melt are referred to as X %NA.

Nanocomposite Isothermal Crystallization and Thermal Behavior

The thermal behavior of the various samples was investigated by differential scanning calorimetry (DSC). DSC traces of quenched samples of the neat polymer and nanocomposites are characteristic of amorphous materials. The addition of CNCs readily increases the T_g of the material from 52°C for the neat polymer up to 63°C for the 17%NA. Figure 1(a) shows the DSC traces of the neat P(D,L-LA) as function of annealing temperature. All traces are dominated by a glass transition around 46–63°C which decreases with annealing (independently of the temperature) and results in a maximum value for samples annealed at 120–130°C. Interestingly most of the DSC traces of the annealed nanocomposites show an auxiliary endothermic peak in the first heating cycle, which appears to correspond to a melting transition (Table I). The annealing process cannot be reproduced in a DSC experiment (lacking pressure) and therefore, crystallization is not visible in cooling cycles, neither in second heating scans. A comparison shows that for all compositions the melting temperature T_m increases with increasing annealing temperature from ~111–124°C in samples annealed at 80°C (0%80°C, 2%80°C, 10%80°C, and 17%80°C) to a maximum of 162°C for sample 17%140°C. Samples 2%140°C and 10%140°C do not show any melting transition. Melting enthalpies were calculated from the area of the peaks present in the first heating cycle of the different samples (Table I). Results show two very different scenarios. At low CNC content, samples show a greater melting enthalpy when annealed at 80–90 and 120°C. These results are in agreement with previously reported data that shows the ability of the polymer to form two different crystal structures, α' and α, when crystallized isothermally at temperatures between 80 and 130°C.[58] These two structures can coexist, resulting in a broadening of the melting peak. Crystallization of the loosely packed α' form is already visible in the neat P(D,L-LA) when annealed at 80°C, showing a broad melting peak at 124°C which accounts for the highest associated enthalpy. Crystallization of the polymer into more densely

Table I. Glass Transition Temperature (T_g), Melting Enthalpy, and Corresponding Transition Temperature of Neat P(D,L-LA) and P(D,L-LA)/CNC Nanocomposites Containing the Indicated Amount of CNCs Calculated from DSC Thermograms Shown in Figure 1 as Function of the CNC Content and the Annealing Temperature

	T_g (°C)/Melting enthalpy (J g^{-1})/transition temperature (°C)			
Annealing temperature (°C)	0 wt % CNC	2 wt % CNC	10 wt % CNC	17 wt % CNC
NA	52/0.0/n.d.	61/0.0/n.d.	63/0.0/n.d.	63/0.0/n.d.
80	56/11.8/124	47/3.0/113	54/2.6/119	50/9.1/111
90	49/0.0/n.d.	46/3.4/120	64/2.4/127	47/7.0/117
100	53/0.0/n.d.	49/1.8/124	54/1.6/131	49/6.1/126
110	47/0.0/n.d.	46/2.6/135	51/0.7/139	48/5.2/130
120	54/0.0/n.d.	61/2.8/145	57/6.1/150	52/2.3/142
130	50/0.0/n.d.	59/1.4/150	64/1.4/152	50/1.8/152
140	62/0.0/n.d.	53/0.0/n.d.	53/0.0/n.d.	52/0.7/162

n.d. = not detectable, NA = not annealed, quenched from the melt.

packed structures is only possible for samples containing CNCs. At higher CNC content (17 wt %), when the rod-shaped nanocrystals form a percolating network,[40,44,59] the melting enthalpy decreases with increasing annealing temperature. This effect could be explained by the reduced mobility of the polymer chains when confined by the CNC network thus, frustrating the ordered arrangement of the chains. Furthermore, the melting temperatures of annealed samples containing high CNC content (17 wt %) are lower than their counterparts at lower CNC content (10 wt %), indicating a lower packing density of the polymer chains in the crystal structures. Samples of P(D,L-LA) loaded with 10 wt % CNC show the highest values of melting temperature for all the annealing conditions. At 10 wt % CNC loading ratio and 120°C annealing temperature, a pronounced melting peak at 150°C is visible.

Structure

To probe the structure of the nanocomposites, X-ray diffraction patterns of the series containing 10 wt % CNCs (Figure 2) were acquired. This composition was chosen for its higher melting

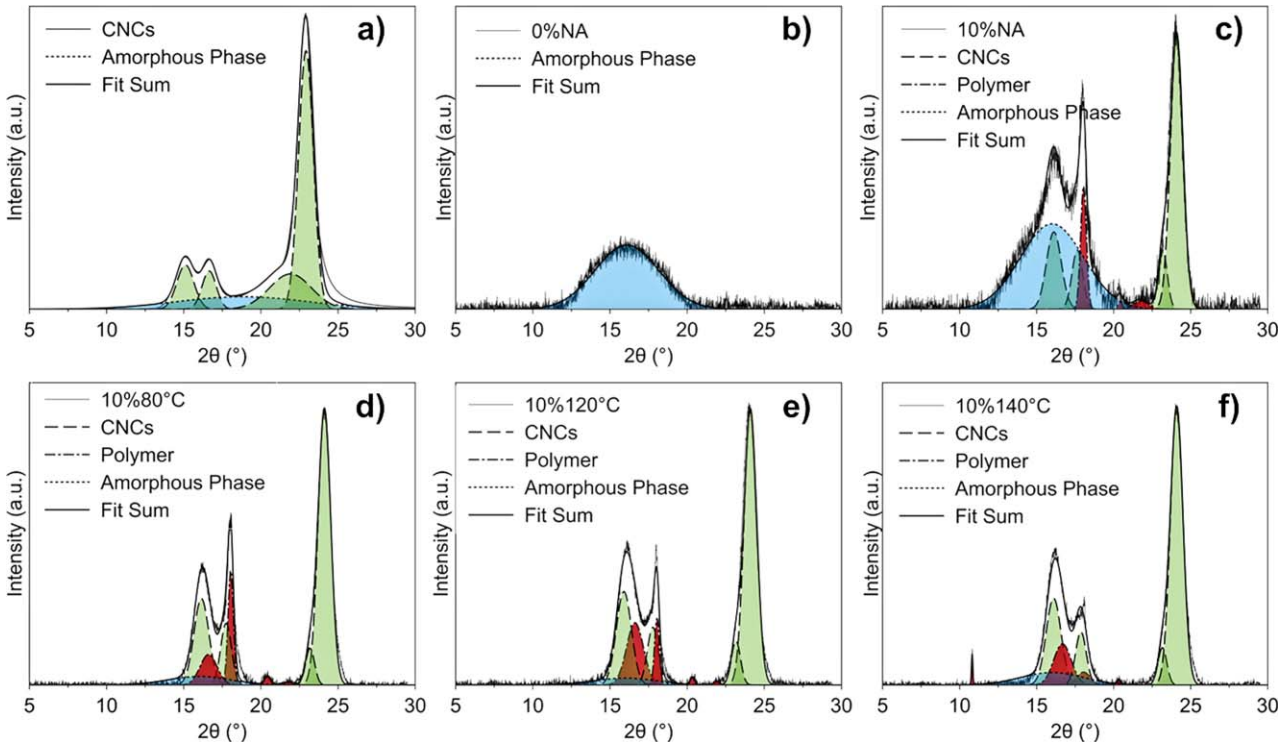

Figure 2. X-ray diffraction patterns of cellulose nanocrystals (a), a film of the quenched neat P(D,L-LA) (0% NA, b), and films of the P(D,L-LA)/CNC nanocomposites containing 10 wt % CNCs as prepared (10%NA, c) and annealed at 80°C (10%80°C, d), 120°C (10%120°C, e), and 140°C (10%140°C, f) for 90 min. The contribution of cellulose diffraction peaks are labeled in green, contribution of polymer s in red and the amorphous phase in blue. [Color figure can be viewed in the online issue, which is available at wileyonlinelibrary.com.]

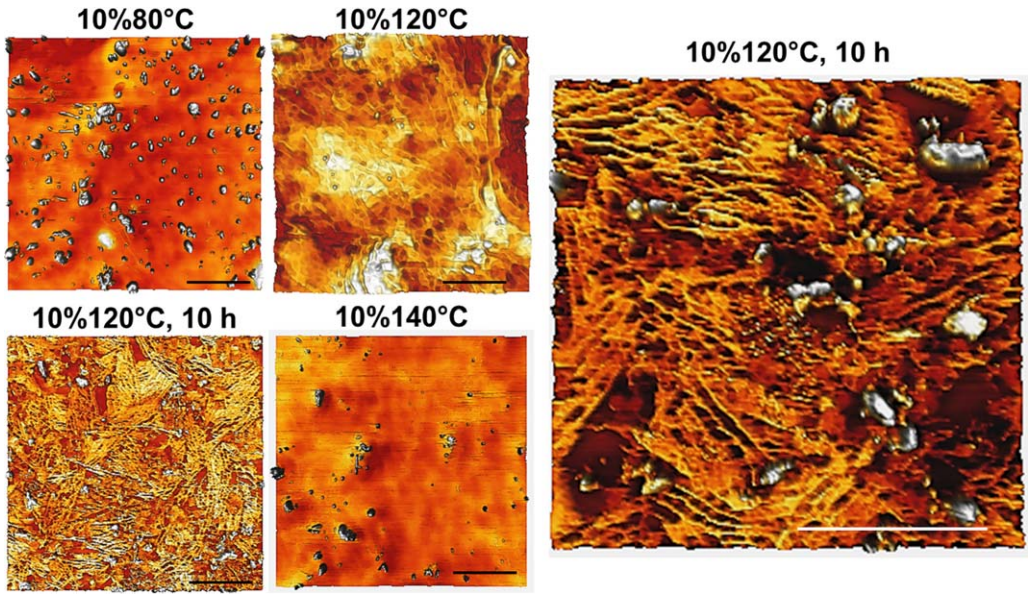

Figure 3. AFM phase 3D images of P(D,L-LA)/CNC nanocomposite films containing 10 wt % CNCs annealed at 80, 120, and 140°C for 90 min, and at 120°C for 10 h. Higher magnification image is shown at the right. The scale bar in all micrographs is 500 nm. [Color figure can be viewed in the online issue, which is available at wileyonlinelibrary.com.]

temperature, which is an indication of higher packing density and therefore, higher order of the polymeric chains. Diffraction patterns of the neat nanocrystals [Figure 2(a)] and of the quenched neat copolymer without CNCs [Figure 2(a)] are included for the purpose of comparison. [Figure 2(a)] shows the typical diffraction pattern of cellulose I with diffraction peaks at $2\theta = 16.1°$, 17.6°, 23.1°, and 24.09° corresponding to the (101), (10 ī), (021), and (002) crystalline planes respectively. [Figure 2(b)] shows the characteristic halo of a purely amorphous material at a $2\theta = 16°$.

The diffractogram of the quenched nanocomposite [Figure 2(c)] reveals that the introduction of CNCs readily promotes the crystallization of the polymer as can be seen from the presence of the characteristic reflections of the (200)/(110) and (203) planes.[57] Although a significant amount of amorphous polymer is still present, the potential of CNCs to induce crystallization in an amorphous polymer is surprising. Isothermal crystallization at 80°C reduces significantly the amorphous content and a predominant α' crystal form can be deduced by the absence of the reflection peaks (103) and (010). The α' crystal form is less ordered with a lower packing density and therefore, thermally less stable and mechanically less robust than its counterpart α form. Annealing at 120°C results in further decrease of the amorphous phase, thus confirming the recorded DSC traces. At this isothermal crystallization temperature the formation of an α- structure is expected but no presence of the minor reflections is observed. By contrast, the appearance of a peak at $2\theta = 16.5°$ in all annealed samples suggests the presence of a different crystal structure or ordering of the copolymer. Stoclet et al.[24] have previously assigned this Bragg peak to the formation of a mesophase, proposing that small amounts of the D-isomer introduce flexibility to the copolymer chain that by folding, excludes it from the crystalline phase. This lamellar structure was determined to appear when neat amorphous P(D,L-LA) containing 4 wt % of the D-isomer was drawn at 70°C applying a minimum of 130% strain. Nevertheless, drawing at higher temperatures induced the formation of a crystalline α form, which shows decreased mechanical properties in comparison to the mesomorphic phase. Interestingly, the P(D,L-LA)/CNC nanocomposite containing 10 wt % CNCs containing a higher percentage of the D-form (11 wt %) studied here is capable of forming this mesomorph. We note that this mesomorph has not been observed in the neat copolymer with the same D-content, indicating that the CNCs play an important role in the structure formation process. Crystallization at higher temperatures, i.e., 140°C, showed coexistence of both, lamellar and α crystalline phases which can be deduced from the appearance of an extra diffraction peak characteristic of the (103) plane at $2\theta \approx 12°$.

Atomic force microscopy phase measurements (Figure 3) show the 10 wt % loaded nanocomposites after compression molding and annealing at different temperatures. Phase images show relative differences in surface hardness of the samples, thus phase separation or fillers within a composite with a sufficient surface hardness difference can be observed. Samples annealed at 80°C show the presence of cellulose nanocrystals inside the copolymer matrix and no lamellar structure can be observed. Some CNCs appear to be lying on the plane of the nanocomposite film while others are oriented at certain angles with respect to this plane and can be observed as dots or smaller ellipsoids. Nanocomposites compression molded at 120°C for 90 min reveal the presence of a lamellar structure that extends over the whole surface and becomes more defined when samples are annealed for 10 h. This finding confirms the presence of a lamellar structure observed by XRD as a diffraction peak at $2\theta = 16.5°$. The lamellar structure incorporates the CNCs within the amorphous phase (Figure 3, zoom-in), suggesting that at least at a content

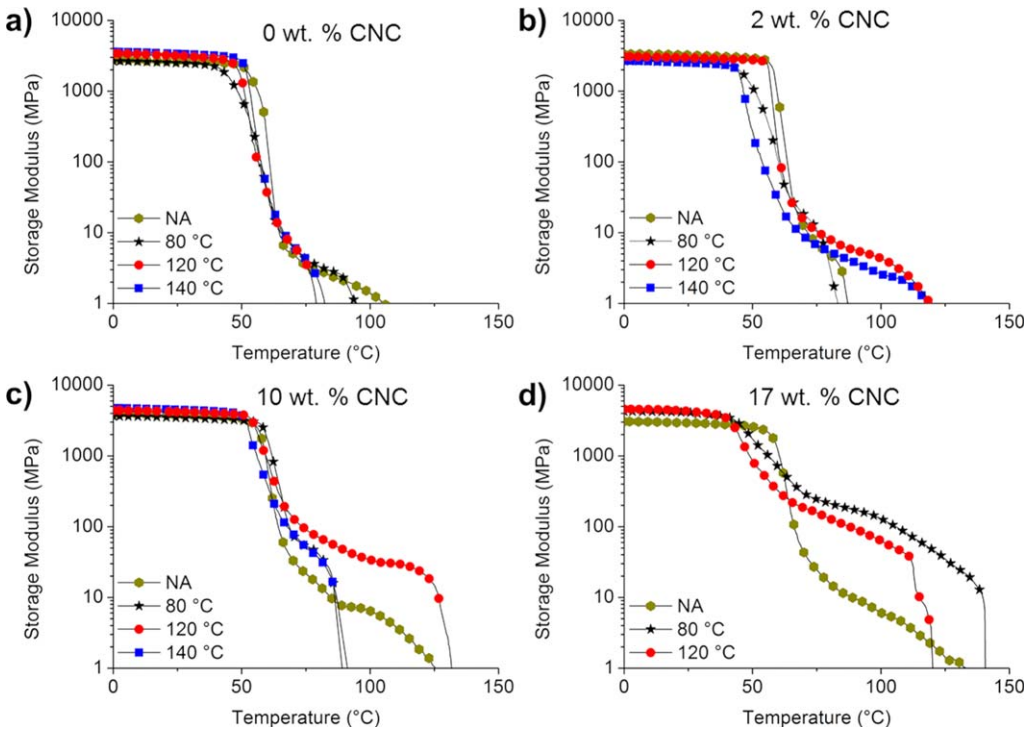

Figure 4. Dynamic mechanical thermal analysis (DMTA) traces of the neat P(D,L-LA) (a) and P(D,L-LA)/CNC nanocomposites containing 2 wt % (b), 10 wt % (c), and 17 wt % CNCs (d). The samples were isothermally annealed at the indicated temperature for 90 min (NA = not annealed). [Color figure can be viewed in the online issue, which is available at wileyonlinelibrary.com.]

of 10 wt %, the CNCs do not disrupt the mesophasic ordering but either induce, or contribute to the formation of the mesophase. Further, annealing at 140°C shows a homogeneous structure that is only altered by the CNCs.

Analysis of these samples by polarized optical microscopy showed familiar birefringence due to the presence of the anisotropic cellulose crystallites but no change was detectable upon annealing (Supporting Information Figure S4).

Mechanical and Dynamic Thermomechanical Properties

The thermomechanical properties of the nanocomposites were studied by dynamic mechanical thermal analysis (DMTA). In the glassy regime, below 50°C, all materials are rigid and display a tensile storage modulus (E') which is independent of the thermal history of the samples but increases with increasing CNC content from 2.9 ± 0.5 GPa for the neat polymer (sample 0%NA) to 4.2 ± 0.1 GPa for the nanocomposite with 17 wt % CNCs (sample 17%80°C). All samples show a steep decrease in the E' upon heating above T_g where many of the samples lose their integrity and fail.

The tensile storage modulus of the different samples above T_g show a clear increase with increasing CNC content. Thus, a neat P(D,L-LA) sample annealed at 120°C displays a lower storage modulus at 80°C (0.3 ± 0.1 MPa) than its counterpart containing 2 wt % CNCs (9.7 ± 4.9 MPa), and this one lower than the 10%120°C (79.1 ± 8.7 MPa) and the 17% 120°C nanocomposites (75.7 ± 8.7 MPa). The reinforcement caused by higher CNC concentration in the 17% 120°C compensates for the reinforcement effect of crystallinity observed in the 10% 120°C samples and thus both samples have similar mechanical properties. In all the CNC containing samples, a clear increase of the mechanical properties is observed upon annealing at 120°C.

Neat P(D,L-LA) samples [Figure 4(a)] show a decreased failure temperature as the annealing temperature increases. Samples quenched from the melt (0%NA) and annealed at 80°C present a higher amount of entanglements that provides them with higher thermomechanical stability. The crystalline fraction of the 0%80°C sample observed by DSC seems to be insufficient to enhance the thermomechanical stability due to low packing density of the α' crystalline form. Samples 0%120°C and 0%140°C, in contrast, have been annealed at a temperature at which the polymer chains have mobility to rearrange reaching a conformation with fewer entanglements and therefore display a lower stability. Samples annealed at 80°C are able to crystallize forming low packing density structures (α' form) even in the absence of CNCs. This effect is reflected on the DMTA traces of samples 2%80°C and 10%80°C as an increase on the crosslinking density (higher mechanical properties in the rubbery plateau) provided by the nanoparticles but showing low thermal stability.

The introduction of CNCs, even at small percentages, induces the crystallization of the copolymer as shown by DSC. Samples annealed at 120°C form a lamellar structure driven by the physical crosslinking of the CNC network with the polymer. The long range ordering of the polymer / CNC network provides to the system with outstanding mechanical properties in the rubbery plateau as well as higher thermal stability. This effect is visible in both, 2% 120°C and 10% 120°C samples, but more

Table II. Averaged Thermomechanical Data ($n > 3$) Obtained from DMTA Experiments for the Neat P(D,L-LA) and P(D,L-LA)/CNC Nanocomposites Containing 2, 10, and 17 wt % CNCs

Sample	E′ at 25°C (GPa)	E′ at 80°C (MPa)	Tg (°C)
0%NA	2.9 ± 0.5	2.7 ± 0.4	63 ± 1
0%80°C	2.5 ± 0.0	3.7 ± 0.3	62 ± 0
0%120°C	2.9 ± 0.2	0.3 ± 0.1	60 ±3
0%140°C	3.1 ± 1.8	1.3 ± 0.5	59 ± 1
2%NA	2.9 ± 0.3	5.1 ± 0.3	65 ± 0
2%80°C	2.5 ± 0.0	6.4 ± 3.1	59 ± 2
2%120°C	3.3 ± 0.4	9.7 ± 4.9	60 ±2
2%140°C	2.5 ± 0.0	5.9 ± 0.6	61 ± 0
10%NA	3.5 ± 0.2	20.5 ± 4.8	65 ± 1
10%80°C	3.3 ± 0.1	48.8 ± 7.7	70 ± 2
10%120°C	3.2 ± 0.7	79.1 ± 8.7	72 ± 2
10%140°C	3.9 ± 0.5	34.3 ± 1.6	65 ± 1
17%NA	3.2 ± 0.3	18.7 ± 3.6	67 ± 1
17%80°C	4.2 ± 0.1	160.7 ± 51.8	64 ± 1
17%120°C	3.9 ± 0.1	75.7 ± 8.7	66 ± 1

T_g values calculated as the maximum in tan δ.

pronounce in the last one, where the thermal stability of the sample annealed at 120°C is 45°C higher than its counterparts [Figure 4(c)]. Indeed, sample 10% 120°C displays a 30 times higher storage modulus in the rubbery plateau (at 80°C) than samples 0%NA (Table III).

Nanocomposites annealed at 140°C form an α form crystal structure [Figure 2(f)] that is thermally more stable than the α′ form. The crystalline fraction of the nanocomposites annealed at 140°C, however, is very low (not detected by DSC) and give as result nanocomposites of increased fragility as the CNC content is increased. Sample 17%140°C was to brittle to be tested by DMTA, breaking always at the beginning of the experiment.

Samples containing 17 wt % CNCs, show a different behavior; with samples annealed at 80°C showing higher dynamic storage modulus above the T_g which is indeed in agreement with the DSC traces that show a higher crystalline content. Here again, the annealed samples show a higher storage modulus within the rubbery plateau, when compared to the analogous samples quenched from the melt.

Table II summarizes the results obtained by DMTA showing a clear increase of the mechanical properties of the nanocomposites in the rubbery plateau, as calculated from the plots at 80°C. Additionally to the increase in mechanical properties, an increase in the T_g (maximum in the tan δ) is also observed, which reaches its maxima at 70–72°C for samples loaded with 10 wt % CNC and annealed at 80 and 120°C. This implies the possibility of exploiting this biocopolymer at higher temperatures having still, mechanical stability.

The mechanical properties of the materials were also studied by tensile testing (Figure 5) and the results are summarized in

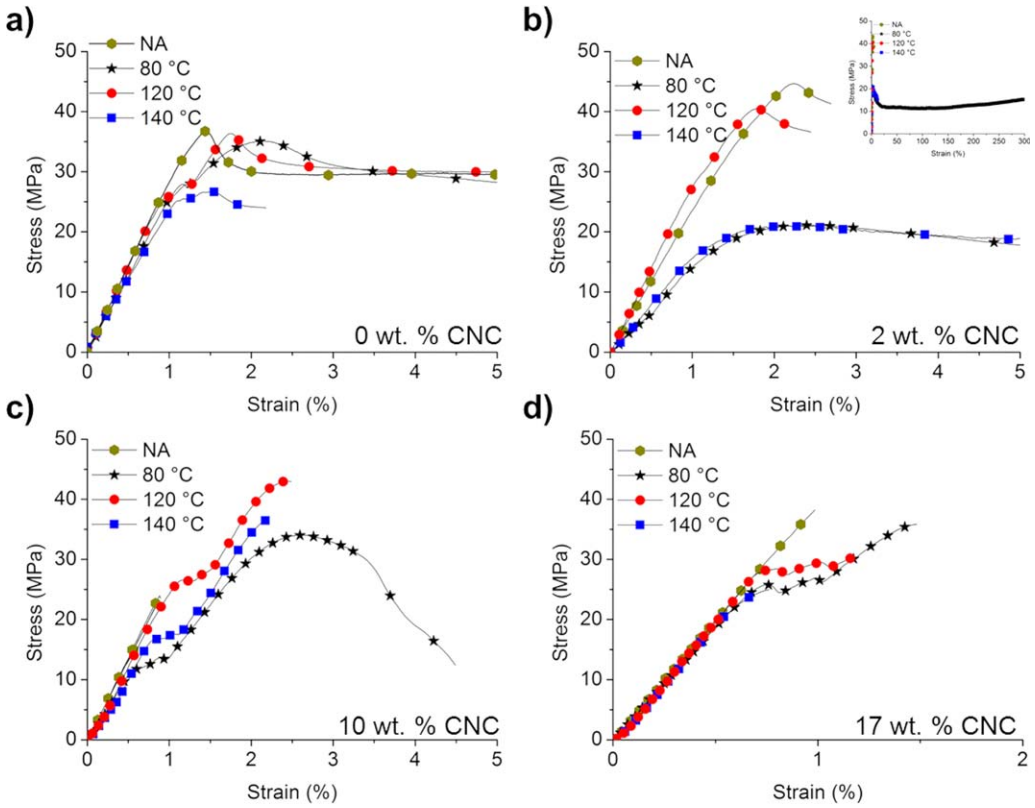

Figure 5. Stress–strain curves of the neat neat P(D,L-LA) (a) and P(D,L-LA)/CNC nanocomposites containing 2 wt % (b), 10 wt % (c), and 17 wt % CNCs (d). The samples were isothermally annealed at the indicated temperature for 90 min (NA = not annealed). [Color figure can be viewed in the online issue, which is available at wileyonlinelibrary.com.]

Table III. Averaged Mechanical Data ($n > 3$) Obtained from Stress–Strain Experiments at Room Temperature for the Neat P(D,L-LA) and P(D,L-LA)/CNC Nanocomposites Loaded with 2, 10, and 17 wt % CNCs

Sample	*E* (GPa)	Yield strength (MPa)	Ultimate strength (MPa)	Max. strain (%)
0%NA	2.7 ± 0.3	36.8 ± 2.3	30.3 ± 3.1	16 ± 4
0%80°C	2.6 ± 0.2	25.7 ± 2.1	36.9 ± 1.8	65 ± 63
0%120°C	3.1 ± 0.2	27.6 ± 1.5	39.1 ± 2.8	14 ± 0
0%140°C	2.8 ± 0.5	31.6 ± 6.5	32.4 ± 5.7	2 ± 0
2%NA	2.5 ± 0.1	46.6 ± 2.6	41.5 ± 1.8	4 ± 1
2%80°C	1.0 ± 0.3	17.0 ± 5.1	16.7 ± 1.8	213 ± 137
2%120°C	3.4 ± 0.4	42.8 ± 5.6	38.4 ± 4.4	3 ± 1
2%140°C	1.4 ± 0.3	19.2 ± 3.8	2.4 ± 1.4	15 ± 6
10%NA	2.8 ± 0.2	33.3 ± 8.5	33.3 ± 8.5	1.2 ± 0.3
10%80°C	3.5 ± 0.1	24.7 ± 0.4	36.8 ± 1.9	1.8 ± 0.2
10%120°C	3.8 ± 0.3	27.8 ± 1.9	42.2 ± 0.0	1.8 ± 0.0
10%140°C	4.0 ± 0.2	32.8 ± 3.9	37.9 ±2.6	1.4 ± 0.0
17%NA	3.7 ± 0.3	41.8 ± 3.1	41.8 ± 3.1	1.2 ± 0.2
17%80°C	4.0 ± 0.3	27.9 ± 0.0	41.23 ± 3.2	1.6 ± 0.1
17%120°C	4.1 ± 0.2	28.1 ± 0.9	30.72 ± 0.0	1.2 ± 0.0
17%140°C	4.1 ± 0.9	27.7 ± 0.9	27.7 ± 0.9	0.7 ± 0.2

Table III. Stress-strain curves show an increase of the Young's modulus and ultimate strength upon introduction of CNCs and after annealing, while the elongation at break is reduced. This is a clear indication of the stiffening of the samples as they crystallize and are reinforced through a rigid filler.

Samples annealed at 80°C show, independently of the CNC content, the highest elongation at break, proving again that the crystal structure formed at this temperature is loosely packed and therefore mechanically less robust. However, samples annealed at 120°C display the highest Young modulus values when compared to composites with equal CNC content but different thermal treatment. This is again an indication of the annealing temperature effect (at 120°C) in the nanocomposites, which promotes a long range ordering that provides to the material with higher cohesion. A similar trend is observed when analyzing the ultimate strength, with samples annealed at 120°C showing the highest values. The highest ultimate strength was observed in samples loaded with 10 wt % CNCs annealed at 120°C.

CONCLUSIONS

Cellulose nanoparticles introduced into P(D,L-LA) copolymer matrices not only reinforce the material increasing the mechanical properties but also serve to nucleate the crystallization of the copolymer, originally amorphous. DSC data supports this statement, showing melting peaks for the samples containing CNCs and annealed at temperatures between 80 and 130°C. Two different scenarios can be distinguished, at low CNC loading ratio crystallization is more pronounced at 80–90°C and 120°C, supporting the hypothesis of the preferential formation of α and α' structures while at higher CNC content, when the nanoparticles form dense percolation networks, crystallization is hindered by the reduced mobility of the copolymer chains that appear to be confined within the network. The highest and more pronounced single melting peak was found at 10 wt % CNC loading and 120°C annealing temperature. Crystallization was confirmed by XRD where a clear decrease of the amorphous phase is observed in the annealed samples. Furthermore, spectra suggest the formation of a predominant α' structure at low annealing temperatures while at high temperatures α structure is the predominant. The presence of a mesophase was observed by XRD spectra and confirmed by AFM measurements in which a clear lamella was observed when samples were annealed at 120°C for 10 h.

The influence of the observed crystallization effects and CNC reinforcement on the thermomechanical properties of the materials were investigated with a range of experimental techniques. While low CNC loading ratios lead to minor increase of the thermomechanical properties, loading ratios of 10 wt % or higher lead to a clear reinforcement above the glass transition temperature up to 50°C. Nanocomposites reinforced with 10 wt % CNC and annealed at 120°C for 90 min show the best combination of mechanical and thermomechanical properties, supporting the idea that the formation of a mesophase increases the thermal stability of the material.

The combined effects of stress-transfer via the CNC percolating network and of lamellar formation gives rise to an interesting combination of thermomechanical properties that will allow for an extent range of exploitation of P(D,L-LA) copolymers. Most importantly, the application of these conditions (addition of CNCs and annealing at 120°C) to semicrystalline polylactides (D : L ratio < 11 : 89) will probably extend the thermal range of application and reduce the crystallization time of this biopolymer, thus becoming a more practical polymer in injection molding where pressure and stress are applied.

ACKNOWLEDGMENTS

The authors gratefully acknowledge funding from the Swiss National Science foundation (National Research Programme 64, Project #406440_131264/1) and the Adolphe Merkle Foundation. Authors also thank Dr. Roy Trittschak for help and discussions with XRD experiments.

REFERENCES

1. Drumright, R. E.; Gruber, P. R.; Henton, D. E. *Adv. Mater.* **2000**, *12*, 1841.
2. Nampoothiri, K. M.; Nair, N. R.; John, R. P. *Bioresoure Technol.* **2010**, *101*, 8493.
3. Vieira, M. G. A.; da Silva, M. A.; dos Santos, L. O.; Beppu, M. M. *Eur. Polym. J.* **2011**, *47*, 254.
4. Yu, L.; Dean, K.; Li, L. *Prog. Polym. Sci.* **2006**, *31*, 576.
5. Bopp, R.; Whelan, J. Method for Producing Semicrystalline Polylactic Acid Articles; US Patent 20030068405 A1, **2003**.
6. Auras, R.; Harte, B.; Selke, S. *Macromol. Biosci.* **2004**, *4*, 835.
7. Weber, C. J.; Haugaard, V.; Festersen, R.; Bertelsen, G. *Food Addit. Contam.* **2002**, *19*, 172.
8. Ulery, B. D.; Nair, L. S.; Laurencin, C. T. *J. Polym. Sci. B Polym. Phys.* **2011**, *49*, 832.
9. Rhim, J.-W.; Park, H.-M.; Ha, C.-S. *Prog. Polym. Sci.* **2013**, *38*, 1629.
10. Ovitt, T. M.; Coates, G. W. *J. Am. Chem. Soc.* **1999**, *121*, 4072.
11. Zhong, Z. Y.; Dijkstra, P. J.; Feijen, J. *J. Am. Chem. Soc.* **2003**, *125*, 11291.
12. Zhong, Z. Y.; Dijkstra, P. J.; Feijen, J. *Angew. Chem. Int. Ed.* **2002**, *41*, 4510.
13. Perego, G.; Cella, G. D.; Bastioli, C. *J. Appl. Polym. Sci.* **1996**, *59*, 37.
14. Liu, Y.; Wang, L.; He, Y.; Fan, Z.; Li, S. *Polym. Int.* **2010**, *59*, 1616.
15. Mano, J. F.; Wang, Y. M.; Viana, J. C.; Denchev, Z.; Oliveira, M. J. *Macromol. Mater. Eng.* **2004**, *289*, 910.
16. Zhang, J. M.; Duan, Y. X.; Sato, H.; Tsuji, H.; Noda, I.; Yan, S.; Ozaki, Y. *Macromolecules* **2005**, *38*, 8012.
17. Desantis, P.; Kovacs, A. J. *Biopolymers* **1968**, *6*, 299.
18. Hoogsteen, W.; Postema, A. R.; Pennings, A. J.; Ten Brinke, G.; Zugenmaier, P. *Macromolecules* **1990**, *23*, 634.
19. Eling, B.; Gogolewski, S.; Pennings, A. J. *Polymer* **1982**, *23*, 1587.
20. Ikada, Y.; Jamshidi, K.; Tsuji, H.; Hyon, S. H. *Macromolecules* **1987**, *20*, 904.
21. Schmidt, S. C.; Hillmyer, M. A. *J. Polym. Sci. B Polym. Phys.* **2001**, *39*, 300.
22. Dorgan, J. R.; Braun, B. Polymer Composites Incorporating Stereocomplexation; US Patent 20110319509 A1, **2011**.
23. Anderson, K. S.; Hillmyer, M. A. *Polymer* **2006**, *47*, 2030.
24. Stoclet, G.; Seguela, R.; Lefebvre, J. M.; Elkoun, S.; Vanmansart, C. *Macromolecules* **2010**, *43*, 1488.
25. Stoclet, G.; Seguela, R.; Vanmansart, C.; Rochas, C.; Lefebvre, J. M. *Polymer* **2012**, *53*, 519.
26. Stoclet, G.; Seguela, R.; Lefebvre, J. M.; Rochas, C. *Macromolecules* **2010**, *43*, 7228.
27. Pluta, M.; Galeski, A. *Biomacromolecules* **2007**, *8*, 1836.
28. Nam, J. Y.; Ray, S. S.; Okamoto, M. *Macromolecules* **2003**, *36*, 7126.
29. Ray, S. S.; Bousmina, M. *Prog. Mater. Sci.* **2005**, *50*, 962.
30. Liao, R.; Yang, B.; Yu, W.; Zhou, C. *J. Appl. Polym. Sci.* **2007**, *104*, 310.
31. Raquez, J.-M.; Habibi, Y.; Murariu, M.; Dubois, P. *Prog. Polym. Sci.* **2013**, *38*, 1504.
32. Barrau, S.; Vanmansart, C.; Moreau, M.; Addad, A.; Stoclet, G.; Lefebvre, J. M.; Seguela, R. *Macromolecules* **2011**, *44*, 6496.
33. Braun, B.; Dorgan, J. R.; Hollingsworth, L. O. *Biomacromolecules* **2012**, *13*, 2013.
34. De Souza Lima, M. M.; Wong, J. T.; Paillet, M.; Borsali, R.; Pecora, R. *Langmuir* **2002**, *19*, 24.
35. Šturcová, A.; Davies, G. R.; Eichhorn, S. J. *Biomacromolecules* **2005**, *6*, 1055.
36. Rusli, R.; Eichhorn, S. J. *Appl. Phys. Lett.* **2008**, *93*, 033111.
37. Araki, J.; Wada, M.; Kuga, S. *Langmuir* **2001**, *17*, 21.
38. Habibi, Y.; Lucia, L. A.; Rojas, O. J. *Chem. Rev.* **2010**, *110*, 3479.
39. Mueller, S.; Weder, C.; Foster, E. J. *RSC Adv.* **2014**, *4*, 907.
40. Camarero Espinosa, S.; Kuhnt, T.; Foster, E. J.; Weder, C. *Biomacromolecules* **2013**, *14*, 1223.
41. Capadona, J. R.; Shanmuganathan, K.; Tyler, D. J.; Rowan, S. J.; Weder, C. *Science* **2008**, *319*, 1370.
42. Coulibaly, S.; Roulin, A.; Balog, S.; Biyani, M. V.; Foster, E. J.; Rowan, S. J.; Fiore, G. L.; Weder, C. *Macromolecules* **2013**, *47*, 152.
43. Biyani, M. V.; Foster, E. J.; Weder, C. *ACS Macro Lett* **2013**, *2*, 236.
44. Jorfi, M.; Roberts, M. N.; Foster, E. J.; Weder, C. *ACS Appl. Mater. Interfaces* **2013**, *5*, 1517.
45. Kumar, S.; Hofmann, M.; Steinmann, B.; Foster, E. J.; Weder, C. *ACS Appl. Mater. Interfaces* **2012**, *4*, 5399.
46. Capadona, J. R.; Van Den Berg, O.; Capadona, L. A.; Schroeter, M.; Rowan, S. J.; Tyler, D. J.; Weder, C. *Nat. Nanotechnol.* **2007**, *2*, 765.
47. Tang, L.; Weder, C. *ACS Appl. Mater. Interfaces* **2010**, *2*, 1073.
48. Pei, A.; Zhou, Q.; Berglund, L. A. *Compos. Sci. Technol.* **2010**, *70*, 815.
49. Fortunati, E.; Armentano, I.; Zhou, Q.; Puglia, D.; Terenzi, A.; Berglund, L. A.; Kenny, J. M. *Polym. Degrad. Stab.* **2012**, *97*, 2027.
50. Goffin, A.-L.; Raquez, J.-M.; Duquesne, E.; Siqueira, G.; Habibi, Y.; Dufresne, A.; Dubois, P. *Biomacromolecules* **2011**, *12*, 2456.

51. Habibi, Y.; Aouadi, S.; Raquez, J.-M.; Dubois, P. *Cellulose* **2013**, *20*, 2877.

52. Raquez, J. M.; Murena, Y.; Goffin, A. L.; Habibi, Y.; Ruelle, B.; DeBuyl, F.; Dubois, P. *Compos. Sci. Technol.* **2012**, *72*, 544.

53. Dorgan, J. R.; Hollingsworth, L. O. Sustainable Polymeric Nanocomposites; US Patent 20080118765 A1, **2008**.

54. Dong, X. M.; Gray, D. G. *Langmuir* **1997**, *13*, 3029.

55. Johnson Ford, E. N. *J. Eng. Fiber. Fabr.* **2010**, *5*, 10.

56. Correa, A. C.; Teixeira, E. D. M.; Pessan, L. A.; Capparelli Mattoso, L. H. *Cellulose* **2010**, *17*, 1183.

57. Stoclet, G.; Seguela, R.; Lefebvre, J. M.; Li, S.; Vert, M. *Macromolecules* **2011**, *44*, 4961.

58. Saeidlou, S.; Huneault, M. A.; Li, H.; Park, C. B. *Prog. Polym. Sci.* **2012**, *37*, 1657.

59. Eichhorn, S. J.; Dufresne, A.; Aranguren, M.; Marcovich, N. E.; Capadona, J. R.; Rowan, S. J.; Weder, C.; Thielemans, W.; Roman, M.; Renneckar, S.; Gindl, W.; Veigel, S.; Keckes, J.; Yano, H.; Abe, K.; Nogi, M.; Nakagaito, A. N.; Mangalam, A.; Simonsen, J.; Benight, A. S.; Bismarck, A.; Berglund, L. A.; Peijs, T. J. *Mater. Sci.* **2010**, *45*, 1.